PREDICTION OF AEROELASTIC VIBRATION OF RECTANGULAR CYLINDERS BY k-ε MODEL

By K. Shimada[1] and T. Ishihara[2]

ABSTRACT: The applicability of the k-ε model in the prediction of aerodynamic force and instability is investigated herein. To show that two-dimensional analysis by the k-ε model is different from ordinary two-dimensional analyses that simply neglect the spanwise velocity, an analysis of the aeroelastic vibration of a cross section with $B/D = 2.0$ is performed first using the latter method. In this case, motion-induced vortex oscillation was successfully simulated; however, galloping, in which the flapping motion of the separated shear layer plays an important role, could not be simulated. The result shows that physically reasonable flows can not be obtained by ordinary two-dimensional analyses, unless the spanwise momentum diffusion is incorporated correctly. On the other hand, the k-ε model, which incorporates this diffusion process by an eddy viscosity, enables two-dimensional analyses even in the high Reynolds number region. In this paper, applicability of the model is examined for rectangular cross sections with a wide range of B/D ratio, i.e., $0.6 \leqq B/D \leqq 8.0$. Various typical aerodynamic features calculated using this model were found to be in good agreement with those obtained experimentally, particularly including discontinuities in Strouhal number at the critical cross sections of $B/D = 2.8$ and 6.0. Based on this result, an elastically supported $B/D = 2.0$ cylinder was analyzed. The motion-induced vortex oscillation and a coupling of the vortex-induced oscillation and galloping were successfully simulated, and their values were in good agreement with those measured in experiments conducted earlier.

INTRODUCTION

Since an elongated rectangular cross section is a common and basic configuration found in many structures, such as tall buildings and bridges, it is important in terms of their aerodynamic design to investigate in detail the aerodynamic characteristics of cylinders with rectangular cross section. In bodies with such cross sections, the separated shear layer, which is generated at the leading edge, plays an important role in the production of aerodynamic forces. The behavior of the shear layer separated from the windward corner and vortices shedding into the wake is dependent on the B/D ratio, where B = length along the direction of flow and D = depth of the section. Therefore, it is widely recognized that the drag coefficient, the lift coefficient, and the Strouhal number, which is defined as a periodicity of the shedding vortex, all vary with the B/D ratio (Nakaguchi et al. 1968).

As the aerodynamic behavior of cylinders with a rectangular cross section is characterized by the occurrence of a reattached shear layer, their behavior is classified into two categories, "separated" and "reattached" types, according to the B/D ratio. In "separated-type" cross sections, Karman-type vortex-induced vibration and galloping occur; in "reattached-type" cross sections, motion-induced vortex oscillation and torsional flutter are observed.

Vortex-induced vibration is of particular interest from the practical viewpoint, since it occurs at a relatively lower range of windspeeds. A mathematical model represented by a wake oscillator model was proposed by Tamura and Shimada (1987) for representing the Karman-vortex type of vortex-induced vibrations. However, when it comes to motion-induced vortex oscillations, though prediction of the onset velocity of the excitation is possible (Shiraishi and Matsumoto 1982), there are no effective methods that can predict its response. In recent years, attempts have been made to tackle this kind of high Reynolds number aerodynamic problem, which is involved with large-scale separation and reattachment by means of methods that solve the Navier-Stokes equation numerically.

The numerical procedures presently applied for this purpose are largely classified into two categories. In one, direct numerical simulations are used to solve the Navier-Stokes equation directly; in the second, some type of averaging of the Navier-Stokes equation is performed. The averaged Navier-Stokes equation method is itself classified into one employing a subgrid scale model and another known by its acronym as the RANS (Reynolds-Averaged Navier-Stokes) equation model. Direct numerical simulation and the aforementioned method employing the subgrid scale model are both examples of 3D analyses, and in both methods it is necessary to use at last 10–20 grid points in the direction perpendicular to the flow. One thing common to these methods is that their results are meaningful only when a sufficient spatial resolution is employed; therefore, these methods are memory intensive and require a lot of processing time.

On the other hand, the RANS model enables two-dimensional computations even in flows with high Reynolds numbers. This is possible based upon the hypothesis that, if the spanwise turbulent fluctuation is supposed to be homogeneous, the spatial average of its fluctuation in the spanwise direction is equivalent to its ensemble average. Based on this hypothesis, Franke and Rodi (1991) showed that the Strouhal number and mean drag coefficient of a square cylinder in a smooth flow are reproduced well by an unsteady 2D analysis using the Reynolds stress equation model in combination with a wall function. They also showed that if the conventional standard k-ε model is used in combination with a wall function in an unsteady 2D analysis, vortex shedding is not simulated. Murakami et al. (1990) pointed out that the inability to reproduce vortex shedding is caused by an excessive production of turbulent kinetic energy, which is an artifact of the isotropic eddy viscosity model. To remove this defect, Kato and Launder (1993) used the property of irrotationality of the flow at the impinging region and proposed a modified k-ε model in which production of turbulent kinetic energy is expressed in terms of a vorticity tensor and a velocity strain tensor. They then applied this model to a square cylinder and were able to obtain vastly improved predictions of aerodynamic characteristics and turbulence statistics. Later, Kato (1997) showed that satisfactory results were obtained with respect to the unsteady wind force and vortex-induced vibration of a square cylinder by

[1]Res. Engr., Wind Engrg. Group, Inst. of Technol., Shimizu Corp., 3-4-17 Etchujima, Koto-ku, Tokyo, Japan 135-8530.

[2]Res. Engr., Dr. Engrg., Wind Engrg. Group, Inst. of Technol., Shimizu Corp., 3-4-17 Etchujima, Koto-ku, Tokyo, Japan 135-8530.

Note: Discussion open until March 1, 2000. To extend the closing date one month, a written request must be filed with the ASCE Manager of Journals. The manuscript for this paper was submitted for review and possible publication on March 11, 1999. This paper is part of the ***Journal of Aerospace Engineering***, Vol. 12, No. 4, October, 1999. ©ASCE, ISSN 0893-1321/99/0004-0122–0135/$8.00 + $.50 per page. Paper No. 20467.

using the modified k-ε model combined with a wall function, even with a relatively low spatial resolution. Using the Baldwin-Lomax model, Deng et al. (1994) obtained satisfactory results with respect to aerodynamic and turbulence statistics of a square cylinder. Similarly, Lee (1997) calculated the flow past a square cylinder by using the standard, RNG and the low-Reynolds number k-ε model to evaluate the sensitivity of various parameters such as time accuracy, spatial accuracy, and choice of convection schemes. Bosch and Rodi (1998) made detailed computations using the modified k-ε model by Kato and Launder and discussed various inflow boundary conditions. They showed that the performance of the model could be further improved by the proper inflow boundary condition.

So far, the above applications of the RANS model have been tested only for square cross sections. In the case of rectangular cross sections, there are many aerodynamic phenomena that should be examined from a numerical model point of view. One example of such a phenomenon is the well-known double mode in the lift fluctuation due to unsteady reattachment of the separated shear layer on the side surfaces for cross sections with $2.0 < B/D < 2.8$ (Okajima 1983). Another example is the discontinuities in Strouhal number that are evident at $B/D = 2.8$ and 6.0. Problems like these pose a tremendous challenge to the development of numerical simulation of flow with large-scale separation. Therefore, it is also important for a further development of the RANS model to verify its ability to reproduce these phenomena. In this paper, a modified k-ε model is treated as a representative of the RANS model, and its applicability in simulating the aerodynamic characteristics of stationary rectangular cross sections with B/D ratio lying in the range $0.6 \leqq B/D \leqq 8.0$ in smooth flow is investigated (Shimada and Meng 1998). Then, depending on its suitability, its application to the prediction of the aeroelastic behavior of a $B/D = 2.0$ cross section is discussed. In particular, to show that 2D analysis using the k-ε model is fundamentally different from an ordinary 2D analysis, which simply neglects the spanwise velocity, an analysis by the latter method is demonstrated for comparison.

DIRECT NUMERICAL SIMULATION (CASE1)

Analytical Method

Numerical analysis in CASE1 is based on solving the time-dependent incompressible Navier-Stokes equation, (1)–(2), by the finite-difference method:

$$\mathbf{u}_t + \mathbf{u}\cdot\nabla\mathbf{u} = -p + \mathrm{R}^{-1}\nabla\mathbf{u} \tag{1}$$

$$\nabla\cdot\mathbf{u} = 0 \tag{2}$$

All spatial derivatives are discretized by second-order central differencing except for the convective term. For the convective term, a third-order upwind scheme proposed by Kawamura and Kuwahara (1984) is employed to stabilize the high Reynolds number numerical instability that arises from the nonlinear effect of the convective term:

$$c\frac{\partial u}{\partial x} \approx c\frac{(-u_{i+2} + 8u_{i+1} - 8u_{i-1} + u_{i-2})}{12\Delta x} + |c|\frac{(u_{i+2} - 4u_{i+1} + 6u_i - 4u_{i-1} + u_{i-2})}{4\Delta x} \tag{3}$$

In the time-marching algorithm, which follows the Marker and Cell method originated by Harlow and Welch (1965), the continuum equation is incorporated by solving first the Poisson equation for pressure and subsequently the momentum conservation equations for the respective velocity components using the updated pressure. Time advancement is done by an implicit first-order Euler scheme. In particular, when one considers the simulation to extend to the realm of aeroelastic vibrations, it is necessary to advance the time from about some hundreds to a thousand of the reduced time; therefore, time advancement in an explicit manner is not a reasonable choice. Keeping these points in mind, in the present calculation it was decided to proceed with the calculation in a stable manner so as to be able to simulate vortices that are as large as the Karman vortex, rather than attempt to precisely reproduce the turbulence statistics.

To evaluate the aerodynamic force accurately, the flow structure in the immediate vicinity of the cylinder where steep gradients exist in the physical quantities must be finely resolved, and the behavior of the separated shear layer needs to be captured as correctly as possible. This is achieved by incorporating a generalized curvilinear coordinate system (a body-fitted coordinate system) so as to be able to concentrate a sufficient number of grid points near the boundary.

The physical analytical domain is a circle of $30D$ in radius. The cylinder itself is located slightly upstream ($-5D$) from the center of the domain. The approaching flow is assumed to be smooth and uniform. On the surface of the solid boundary, a no-slip boundary condition is imposed for each velocity component. A Dirichret boundary condition of $p = 0$ is imposed on the remote boundary, and a Neumann boundary condition $\partial p/\partial n = 0$ is imposed on the solid boundary. The Reynolds number is chosen to be $\mathrm{R} = U_\infty D/\nu = 10^4$.

The Runge-Kutta method is used for solving the equation of motion of the cylinder. The Scruton number, which is defined as $Sc = 2m\delta/(\rho_a BD)$, where m, δ, and ρ_a = mass per unit length, logarithmic decrement, and air density, is selected such that its value is 2. Reduced velocity is defined as $Ur = U_\infty/(n_0 D)$, where n_0 = natural frequency of the cylinder. In general, n_0 is fixed in the experiment, but U_∞ is allowed to vary. However, in the analysis, in order to exclude the Reynolds number dependency and to keep the Reynolds number constant, the reduced velocity is adjusted by varying the natural frequency of the cylinder. In the following discussion, two-dimensional and three-dimensional analyses using the CASE1 procedure are referred to as CASE1-2D and CASE1-3D, respectively. In the following section, analysis of the motion-induced vortex oscillation using the two-dimensional analysis scheme of CASE1-2D (Shimada 1995) is described in detail for comparison with the k-ε model (CASE2).

Aeroelastic Vibration of $B/D = 2.0$ Rectangular Cross Section

Flow Pattern around Vibrating Cylinder

The process of vortex formation is of particular interest for understanding the mechanism of vortex-induced vibration. Fig. 1 illustrates a typical pattern of the instantaneous vortical

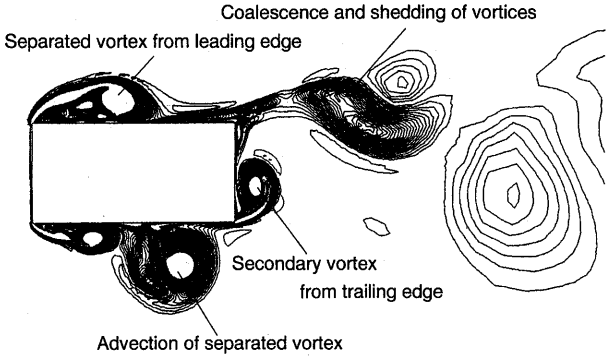

FIG. 1. Vortical Structure around Elastically Supported $B/D = 2.0$ Cross Section in Smooth Flow at Motion-Induced Vortex Oscillation

structure created around a transversely oscillating cylinder. The three primary processes that make up the vortical structure are: (1) formation of the leading edge separation vortex; (2) advection of the vortex along the side surface; and (3) coalescence with the secondary vortex at the trailing edge and shedding of the vortices. Fig. 2 demonstrates the unsteady vorticities during a typical half period of successive oscillation. In the figure, the development process of the separated shear layer is followed by a series of consecutive numbers.

At first, the separated shear layer at the leading edge is enhanced by the transverse oscillation of the cylinder, and vorticity is concentrated gradually in the separation bubble near the leading edge, consequently forming the leading-edge separated vortex (a1–a7). It then travels downstream across the side surface of the cylinder (a8–a9). At this stage, the vorticity is highly concentrated. Concurrently, at the opposite corner of the trailing edge, a secondary vortex is seen to be induced (b1–b5) that coalesces with the advecting vortex in the wake of the cylinder [Fig. 2(e)], at which time, the amplitude of the oscillation reaches almost is maximum value. These merged vortices are then shedded into the wake and form alternate vortex streaks. At the reduced velocity corresponding to Ur = 5.0, which is near the resonant peak of the vortex-induced vibration, the vortex shedding its very stable. This flow formation cycle is completed in one period of oscillation of the cylinder, and the vortex shedding is seen to be almost completely synchronized with the motion of the cylinder.

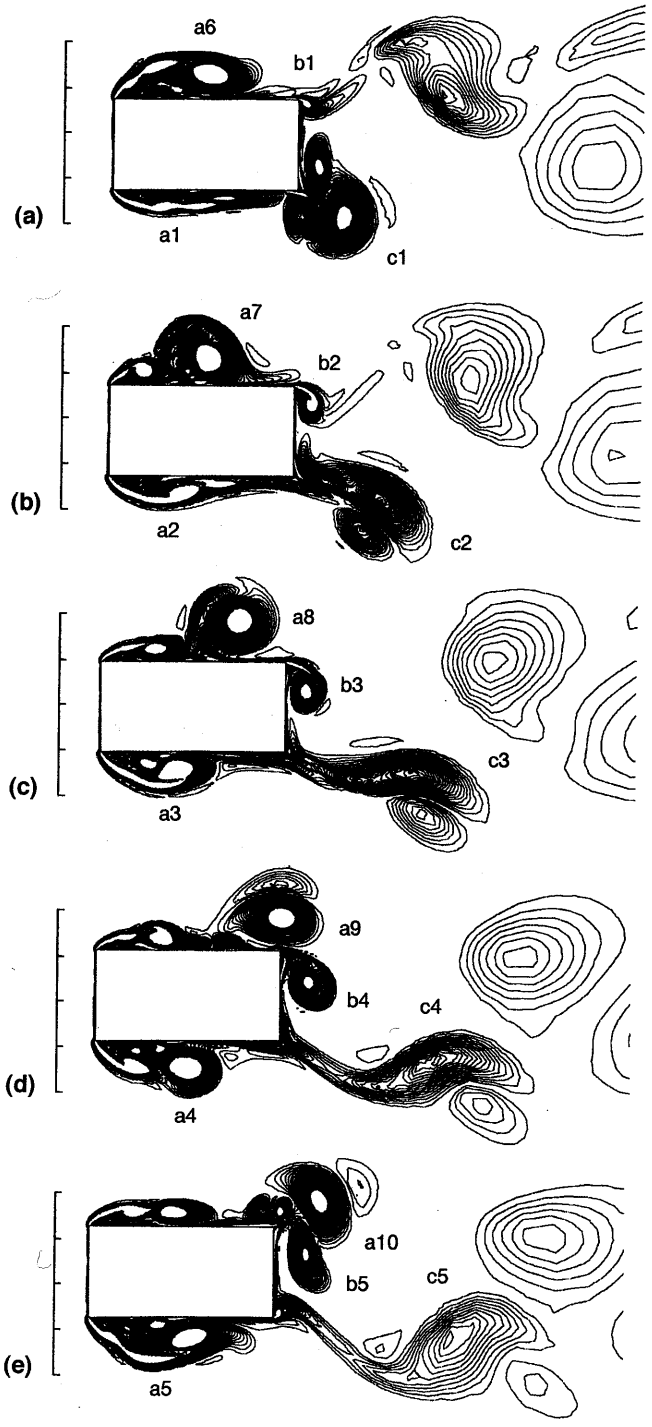

FIG. 2. Vortex Formation Process of Elastically Supported *B/D* = 2.0 Cross Section in Smooth Flow during Half Cycle of Oscillation at *Ur* = 5.0: (a) *t* = 0; (b) *t* = 0.6; (c) *t* = 1.2; (d) *t* = 1.8; (e) *t* = 2.4

Response

Fig. 3 is a comparison of the numerical results obtained using the CASE1-2D procedure and experimental results from various wind tunnel tests that were carried out over a range from Sc = 1.6 to 3.0 (Washizu et al. 1978; Miyazaki 1982; Shiraishi and Matsumoto 1982; Yamada et al. 1982; Utsuno-

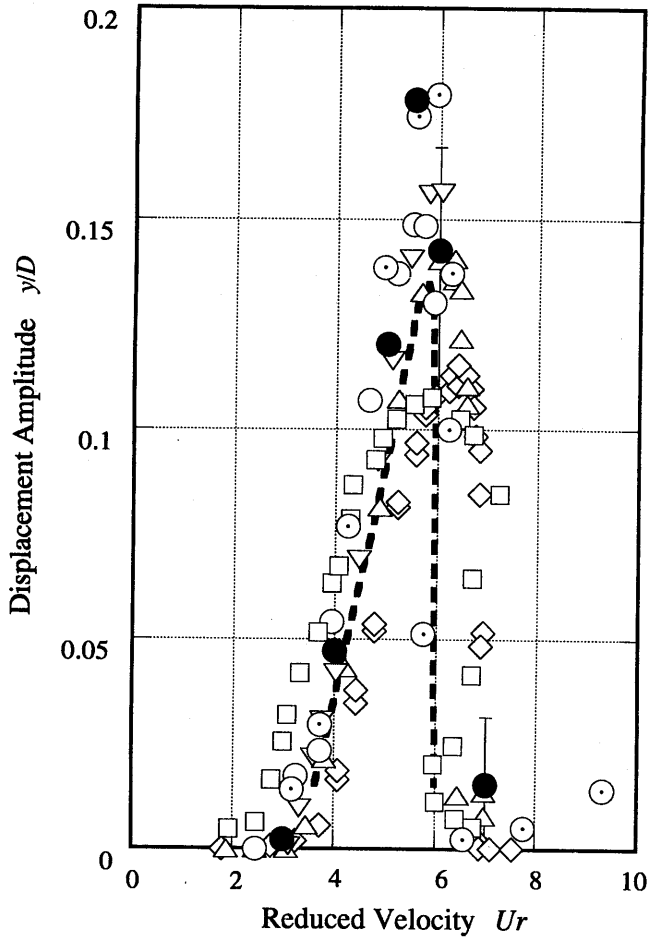

FIG. 3. Motion-Induced Vortex Oscillation of *B/D* = 2.0 Rectangular Cross Section

miya et al. 1984; Takeda and Kato 1992). The large scatter seen in the experimental results can be attributed in large measure to slight differences in the setup conditions of the various tests, for example, the blockage effect and damping. However, all experimental data series show the same tendency; that is, the excitation commences at $Ur = 3.0$, the resonant peak occurs around $Ur = 5.5$, and then the amplitude decreases drastically at $Ur = 7.0$. The computed results are comparable to these experimental results, and the characteristic of the vortex-induced vibration, which is observed over a limited range of reduced velocity, can be recognized.

Unsteady Surface Pressure

Unsteady surface pressure acting on the moving cylinder is usually random, and its two dominant components are the Strouhal component and the natural frequency response component. The latter is primarily important for its contribution to the amplification of vibration. The displacement at $Ur = 5.0$ is seen to be almost sinusoidal. If the displacement is expressed as $y(t) = \Re[Y_0 \exp(i\omega_0 t)]$, where Y_0 and ω_0 = amplitude and circular frequency of the oscillation, the natural frequency response component $Cp_{\tilde{\omega}_0}$ can be decomposed as follows (Washizu et al. 1978):

$$Cp_{\tilde{\omega}_0}(t) = \Re[(Cp_R + iCp_I)\cdot e^{i\tilde{\omega}_0 t}] \tag{4}$$

$$Cp_R = |Cp_{\tilde{\omega}_0}|\cdot\cos\beta_p, \quad Cp_I = |Cp_{\tilde{\omega}_0}|\cdot\sin\beta_p \tag{5}$$

$$|Cp_{\tilde{\omega}_0}| = \sqrt{Cp_R^2 + Cp_I^2}, \quad \beta_p = \tan^{-1}\left(\frac{Cp_I}{Cp_R}\right) \tag{6}$$

The unsteady pressure distributions of the natural frequency response component along the surface of the cylinder are illustrated in Fig. 4. The phase lag β_p and Cp_I are shown in Figs. 4(a and b), respectively. In these figures, the experimental results of forced oscillation by Miyata et al. (1983) and numerical results of forced oscillation by Tamura and Kuwahara (1989) are also shown for comparison. The phase lag β_p obtained using the CASE1-2D procedure varies from a negative value at the windward region to a positive value at the leeward region and is in good agreement with the experimental data. Similarly, the computed Cp_I, which are negative at the windward side and positive at the leeward side of the surface, i.e., the damping force and the excitation force, respectively, are in good agreement with the forced oscillation results.

Simulation of Stationary Rectangular Cylinders

Thus, as shown above, the motion-induced vortex-oscillation can be simulated well even by an ordinary two-dimensional analysis such as the CASE1-2D procedure, in which the spanwise velocity component is simply neglected. This is one of a few cases in which the CASE1-2D procedure works successfully in high Reynolds number problems. In the above case, strong disturbance caused by the enhancement of a vortex at the leading edge makes the flow nearly two-dimensional. However, flow around a body of rectangular cross section is two-dimensional at a relatively low Reynolds number, for which the spanwise momentum transfer seems to be negligible. As the Reynolds number becomes higher, three-dimensionality kicks in. As a result, remedies in numerical procedures to cope with the physical momentum diffusion in the direction of the span are required for these procedures to be realistic. Consequently, prediction of aerodynamic characteristics of stationary cylinders by the CASE1-2D procedure was not successful, nor was the galloping, in which the flapping motion of the separated shear layer plays an important role.

Using one numerical remedy; the CASE1-3D procedure, comparisons are made in Fig. 5 of calculated and observed

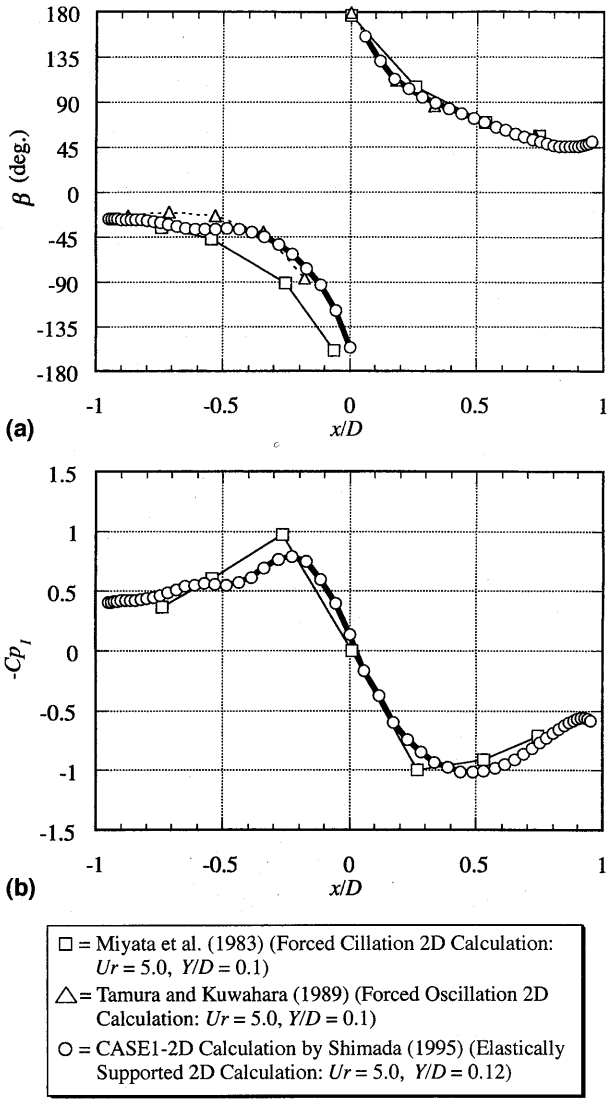

FIG. 4. Unsteady Surface Pressure of $B/D = 2.0$ Rectangular Cross Section: (a) Phase β_p; (b) Cp_I

aerodynamic characteristics of some stationary rectangular cylinders in smooth uniform flow. At $B/D = 3.0$, a discontinuity in the Strouhal number is found to be successfully simulated by the numerical procedure. Fig. 6 shows the instantaneous vorticity ω_z of $B/D = 2.0$ and $B/D = 3.0$ cross sections. In the $B/D = 2.0$ cross section, since the separated shear layer surrounds the body and the Karman vortex is formed in the wake apart from the cross section, the Strouhal number shows small value. On the other hand, in the $B/D = 3.0$ cross section, which demonstrates Strouhal jump, the separated shear layer reattaches onto its side surfaces. The CASE1-3D procedure, which incorporates the spanwise momentum diffusion process, reproduces well these details of the flow. Tamura and Ito (1995, 1997) investigated the aerodynamic characteristics of rectangular cross sections with various B/D ratios using a similar method, and the ability of the procedure has been demonstrated in the literature.

Note that, in general, in the evaluation of aeroelastic vibration it is necessary to perform a calculation by hundreds of reduced time to obtain statistically converging responses. As a consequence, an enormous computational time is required even when using 2D analysis. Therefore, from the point of view of practical use it is not a reasonable choice to perform the computations using 3D direct simulations, since in practical applications it would be required to investigate for various reduced velocities in addition to changing mechanical

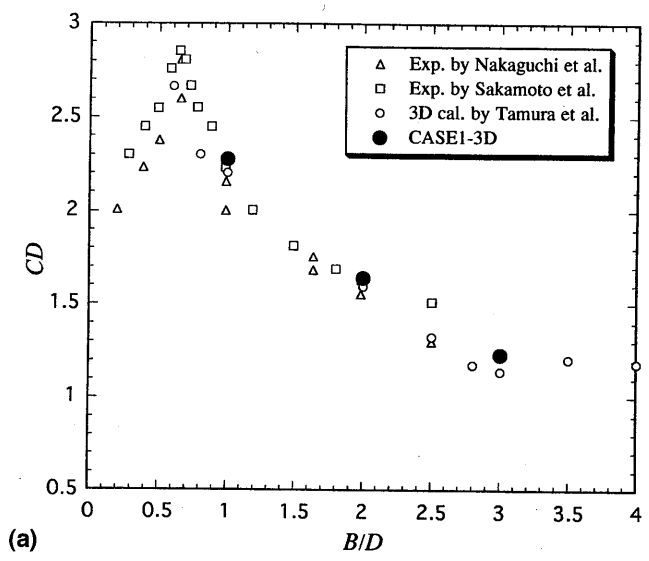

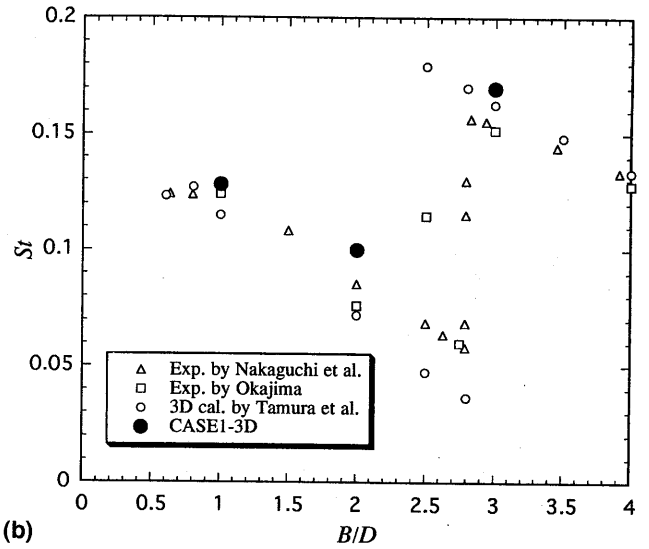

FIG. 5. Aerodynamic Characteristics of Rectangular Cylinders Obtained by 3D Numerical Simulation: (a) Mean Drag Coefficient; (b) Strouhal Number

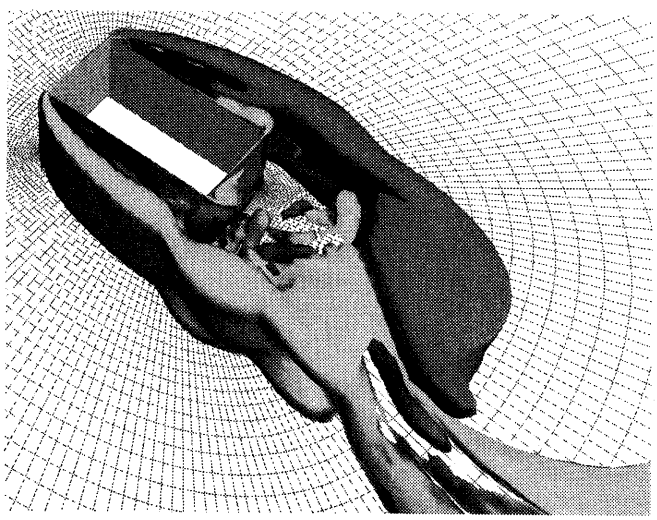

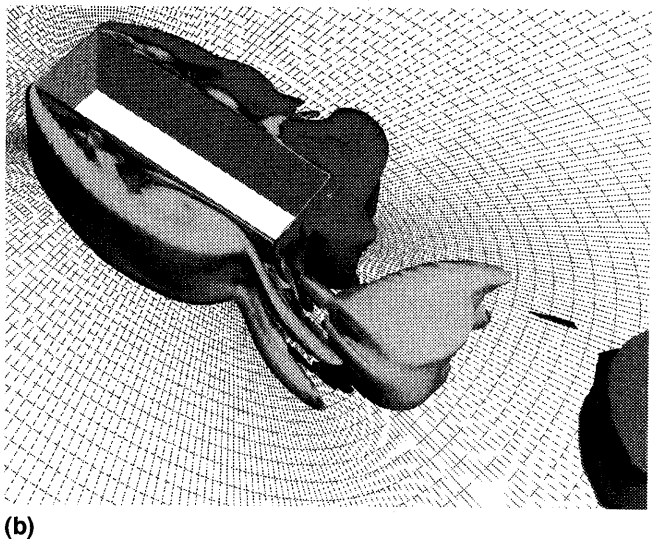

FIG. 6. Vortical Structure (Vorticity ω_z) around Rectangular Cylinders: (a) $B/D = 2.0$; (b) $B/D = 3.0$

properties such as mass-damping ratio. The possibility of reproducing aeroelastic motions of a square cross section by properly incorporating a turbulent diffusion effect was discussed by Kato (1997). Yet so far, most of applications of the RANS model have been confined to square cross sections. In the following, the modified k-ε model by Kato and Launder (1993) is treated as a representative of RANS model, and first, its applicability to stationary cylinders with a wider range of B/D ratio, i.e., $0.6 \leqq B/D \leqq 8.0$ is investigated in detail.

k-ε MODEL (CASE2)

Basic Equation

The Reynolds-averaged incompressible Navier-Stokes equation is expressed as

$$\frac{DU_i}{Dt} = -\frac{\partial}{\partial x_i}\left(P + \frac{2}{3}k\right) + \frac{\partial}{\partial x_j}\left[(\nu + \nu_t)\left(\frac{\partial U_i}{\partial x_j} + \frac{\partial U_j}{\partial x_i}\right)\right] \quad (7)$$

where ν_t = eddy viscosity coefficient and is given as $\nu_t = C_\mu k^2/\varepsilon$. Eq. (7) is reduced to 2D form if the averaging operator $\partial\langle\phi\rangle/\partial x_3 = 0$, which implies that the turbulent fluctuation, which is supposed to be homogeneous in the spanwise direction, is assigned on the equation and then $U_3 = 0$ is substituted.

The turbulent kinetic energy k and its dissipation rate ε are obtained by the following transport equations:

$$\frac{Dk}{Dt} = \frac{\partial}{\partial x_j}\left[\left(\nu + \frac{\nu_t}{\sigma_k}\right)\frac{\partial k}{\partial x_j}\right] + P_k - \varepsilon \quad (8)$$

$$\frac{D\varepsilon}{Dt} = \frac{\partial}{\partial x_j}\left[\left(\nu + \frac{\nu_t}{\sigma_\varepsilon}\right)\frac{\partial \varepsilon}{\partial x_j}\right] + (C_{\varepsilon_1}P_k - C_{\varepsilon_2}\varepsilon)\frac{\varepsilon}{k} \quad (9)$$

The empirical constants in the equation are given as $C_\mu = 0.09$, $C_{\varepsilon_1} = 1.44$, $C_{\varepsilon_2} = 1.92$, $\sigma_k = 1.0$, and $\sigma_\varepsilon = 1.3$, all of which are identical to those used in the conventional standard k-ε model. Since in the case of the standard k-ε model these empirical constants are identified from temporal means of experimentally measured values, justification of their application to the present model in the sense of ensemble averaging is questionable. However, judged from the results, as discussed later, no uncertainties arising from these model constants were observed.

P_k is the production term of turbulent kinetic energy. When the standard k-ε model is used, it is widely recognized that excessive amounts of turbulent kinetic energy are produced near the leading edges of the cross section. In this study, to cope with this defect, a model proposed by Kato and Launder (1993) is employed where

$$P_k = C_\mu \frac{k^2}{\varepsilon} \sqrt{\frac{1}{2}\left(\frac{\partial U_i}{\partial x_j} + \frac{\partial U_j}{\partial x_i}\right)^2} \sqrt{\frac{1}{2}\left(\frac{\partial U_i}{\partial x_j} - \frac{\partial U_j}{\partial x_i}\right)^2} \quad (10)$$

Turbulence Model near Solid Boundary

Treatment of the turbulence model near the boundary is important for a simulation of the flow field around rectangular cylinders that is involved with separation and reattachment. A great many works on the k-ε model have used the wall function near a solid boundary without employing a number of grid points, for reasons of economy. However, the generalized log-law is unsuited for flow with large-scale separation and reattachment (Rodi 1991). Furthermore, if the wall function is used, the effect of the Reynolds number is not precisely reflected. Therefore, the present analysis employs the low Reynolds number one-equation model, which is from here on referred to as the "two-layer model." In other words, the k equation is solved by assigning $k = 0$ on the solid boundary.

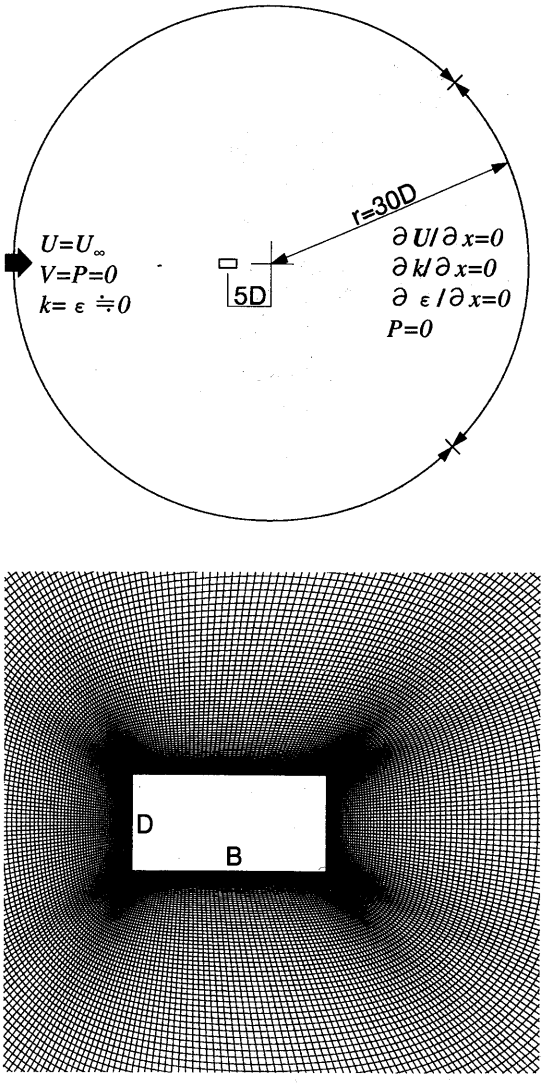

FIG. 7. Analytical Domain and Boundary Conditions and Grid System near Cross Section

TABLE 1. Spatial Resolution

B/D (1)	Grid points (2)
0.6	200 × 200
1.0	200 × 100, 200 × 200
$1.0 < B/D \leqq 8.0$	320 × 200

Instead of solving the ε equation, ε near the wall is determined by the turbulent kinetic energy k using a length scale l_ε. The eddy viscosity, ν_t, in the region where the ε equation is not solved is calculated using the turbulent kinetic energy k and a length l_μ as with ε:

$$\varepsilon = \frac{k^{3/2}}{l_\varepsilon}, \quad \nu_t = C_\mu k^{1/2} l_\mu \quad (11)$$

The length scale l_ε and l_μ are proportional to the turbulent eddy scale $l(= \kappa y)$ and are determined using the following relations:

$$l_\mu = C_l y \left[1 - \exp\left(-\frac{R_y}{A_\mu}\frac{25}{A^+}\right)\right], \quad l_\varepsilon = \frac{C_l y}{1 + 5.3/R_y} \quad (12)$$

where the constants are given as $C_l = \kappa C_\mu^{-3/4}$, $A_\mu = 50.5$, and $A^+ = 25$. In the two-layer model, since l_ε and l_μ are functions of the turbulent Reynolds number $R_y(=k^{1/2}y/\nu)$, the effects of the Reynolds number can be evaluated. The Reynolds number is known to be important for describing the aerodynamic characteristics of bodies with a curved surface, such as a circular cylinder. Numerical studies using the two-layer model conducted by Shimada and Meng (1997) were successful in simulating the variation of the drag force coefficient of a circular cylinder with the Reynolds number. The same approach on a near wall treatment is shown to be effective in a simulation of

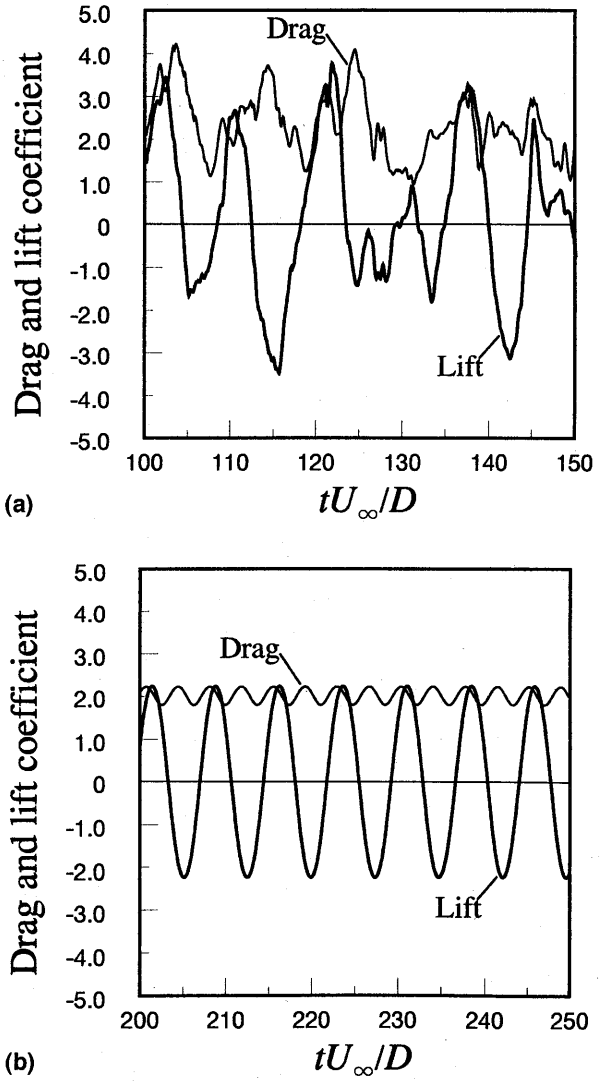

FIG. 8. Time Histories of Drag and Lift Coefficient for Square Cross Section (200 × 100): (a) CASE1-2D (2D Calculation without Turbulence Model); (b) CASE2

the flow past a square prism by Bosch and Rodi (1998). In the present calculation, the two-layer model is applied to the region only within three meshes away from the solid boundary. Also, to evaluate the aerodynamic forces as accurately as possible, the flow structure must be finely resolved in the immediate vicinity of the regions on the cross section. To achieve this, a generalized curvilinear coordinate system is incorporated. The above set of equations is solved by a procedure similar to that presented in the CASE1 calculation, except for the convective terms in the k and ε transport equations, which are discretized by the first-order upwind difference scheme. The analytical domain is a circle with a radius of $30D$, and a rectangular cross section is placed at a distance of $5D$ upstream from the center of the domain, as shown in Fig. 7. The number of grid points used in the runs of calculation are summarized in Table 1.

Fig. 7 also shows the boundary condition. The turbulent kinetic energy and its dissipation rate are $k = 10^{-5}(m^2/s^2)$ and $\varepsilon = 10^{-5}(m^2/s^3)$, respectively. At the outlet boundary, a Neumann-type boundary condition, i.e., $\partial \mathbf{u}/\partial x_1 = 0$ is assigned. The Reynolds number is chosen to be $R = U_\infty D/\nu = 2.2 \times 10^4$ so as to be consistent with the experiment by Lyn (1989), in which turbulent statistics around a square prism were measured in detail.

Verification of Numerical Method ($B/D = 1.0$)

For validation of the general applicability of the two-dimensional approach using the k-ε model and for verification of the present numerical analysis code, its application to a $B/D = 1.0$ cross section that has been investigated in detail both experimentally and numerically is examined. In Fig. 8, time histories of aerodynamic force coefficients obtained by the CASE1-2D analysis, in which simply $u_3 = 0$ is imposed, and those from the calculation employing the turbulence model are illustrated as CASE2. The CASE2 records show an almost sinusoidal periodic fluctuation; however, in CASE1-2D, the fluctuations are random and their amplitudes are quite large. Fig. 9 compares the instantaneous vorticity as calculated by these two methods. In CASE2, an apparent Karman vortex

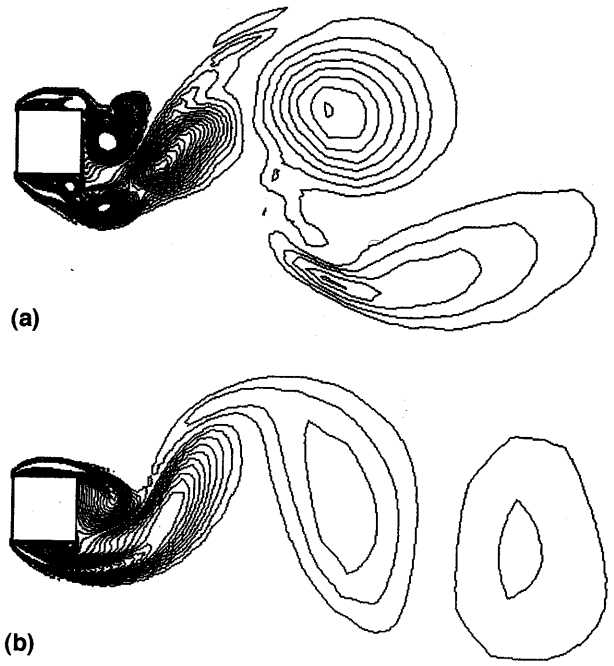

FIG. 9. Instantaneous Vorticity Contour around Square Cross Section (200 × 100): (a) CASE1-2D (2D Calculation without Turbulence Model); (b) CASE2

TABLE 2. Comparison of Aerodynamic Properties

Source (1)	CD (2)	CD' (3)	CL' (4)	St (5)
Franke and Rodi (RSE + w.f.)	2.15	0.383	2.11	0.136
Kato and Launder (M.P. k-ε + w.f.)	2.05 ± 0.03	—	1.16	0.145
Present calculation (200 × 200)	2.05	0.093	1.43	0.141
Sakamoto et al. (Experiment)	2.22	0.132	1.45	0.134

street is formed in the wake of the cross section; however, in CASE1-2D the shedding vortices downstream of the cross section do not advect directly. When an approach similar to CASE1-2D is employed, this kind of defective phenomenon is always observed in the range of Reynolds numbers over 10^4. This is believed to arise from the fact that the momentum that should otherwise be diffused in the spanwise direction by 3D turbulent mixing is unable to diffuse properly using an ordinary 2D procedure, leading to concentrations of extremely strong vorticity like those found in Fig. 9(a). On the other hand, CASE2 incorporates the turbulent diffusive effect adequately and, even at high Reynolds numbers, is successful in simulating smooth periodic vortex shedding by avoiding an excessive concentration of momentum.

In Table 2, aerodynamic force coefficients obtained by the present numerical simulation are compared with some previously obtained numerical results and with the results of an experiment conducted by Sakamoto et al. (1989). With respect to the mean drag coefficient, the results from all the RANS model are in reasonably good agreement with the experimental result, although they are all slightly below the experimental

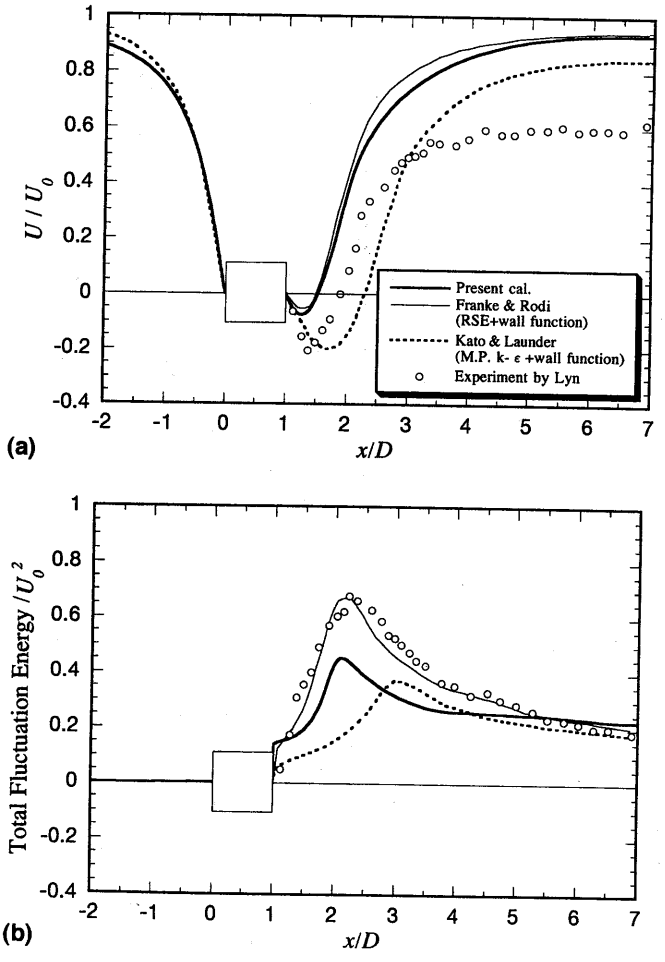

FIG. 10. Distribution of Time Mean Turbulence Statistics on Center Line in Flow of Square Cross Section (200 × 200); (a) U-Component; (b) Total Fluctuation (Periodic Component + Stochastic Component)

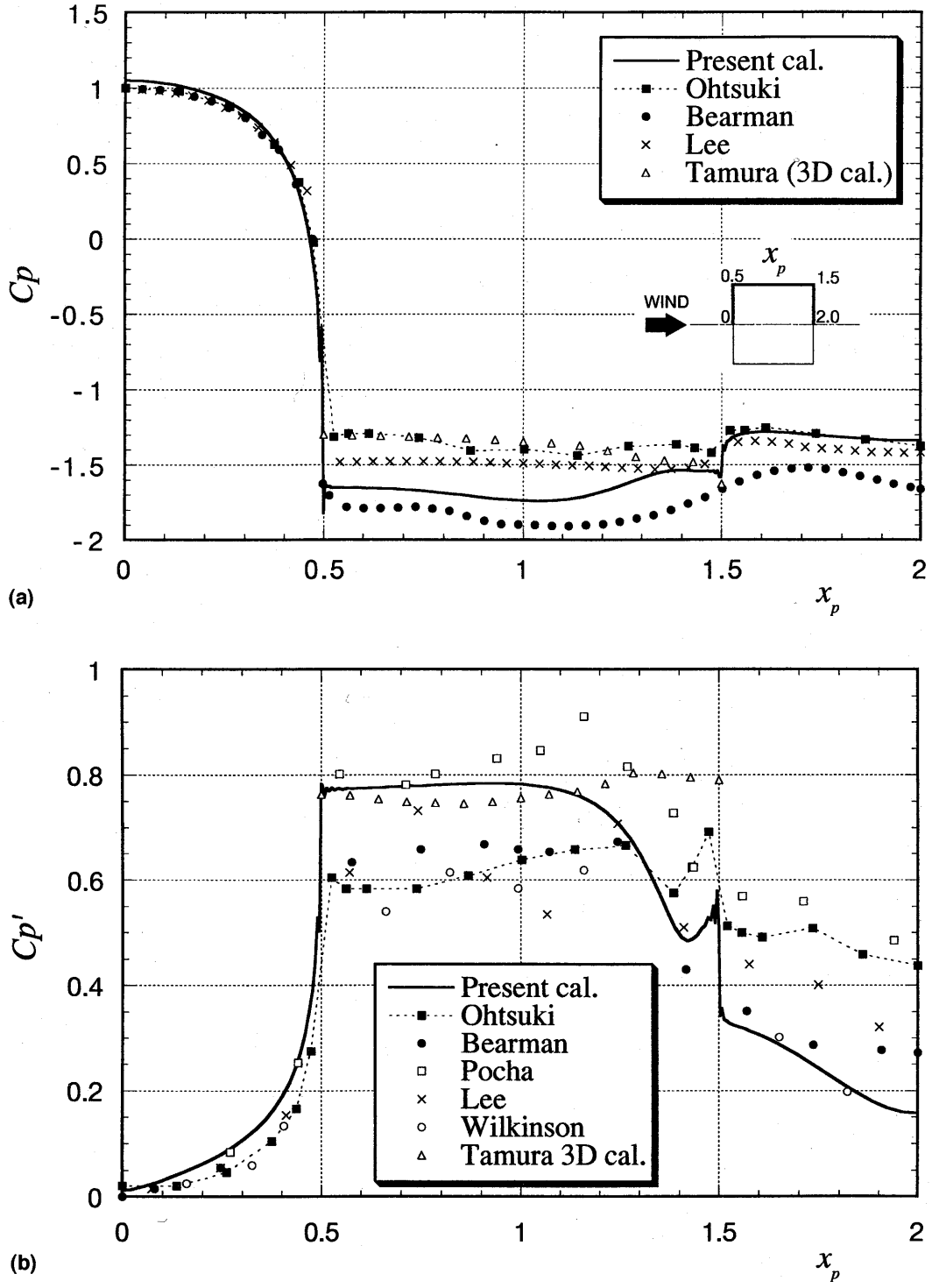

FIG. 11. Pressure Distribution on Square Cross Section: (a) Mean Pressure Distribution; (b) Fluctuating Pressure Distribution

value. However, there are some differences in the fluctuating life coefficient. Arranged in decreasing order of magnitude, the fluctuating lift coefficients line up as follows: Franke and Rodi > the present calculation > Kato and Launder. To account for this difference, the distribution of the mean velocity and of the total fluctuating energy, consisting of both periodic and stochastic components, along the centerline in the wake field is presented in Fig. 10. The size of the reversed flow region formed behind the prism, which is described as a region in which $U/U_\infty < 0$ in Fig. 10(a), as evaluated by the present calculation and by Franke and Rodi, is found to be excessively narrow compared with the experimentally obtained reversed flow region, but that obtained by Kato and Launder is larger. The differences in the estimated size of the reversed flow region can be associated with the differences in magnitude of turbulent mixing in the wake of the prism, which is illustrated as the total fluctuating energy in Fig. 10(b). Franke and Rodi report the largest total fluctuating energy and the highest fluctuation in lift; on the other extreme, Kato and Launder report the lowest total fluctuating energy and the lowest fluctuation in lift. This means that the fluctuation in lift can be related to the turbulent mixing in the wake of the prism and the size of the wake. These observed differences might arise from the differences in the treatment of the turbulence model near the solid boundary and/or the convection scheme. Kato et al. suggested that treatment of the turbulence model near the solid

boundary significantly affects the turbulent statistics, as well as the aerodynamic characteristics.

Fig. 11 shows the distributions of mean and fluctuating pressure coefficients. A square cross section is classified as a separated-type cross section, and its side surfaces are completely immersed in the separated flow region. Therefore, on the side surface, the pressure is suction, and its distribution does not exhibit a large variation. In Fig. 11, although the experimental values are seen to exhibit some amount of scattering in both the mean and the fluctuation coefficients, the present result almost coincides with the experimental results.

Thus, for a stationary square cross section, the modified k-ε model that is incorporated in the present analysis is seen to lead to a satisfactory result with respect to prediction of the aerodynamic statistics, although it provides a rather poor estimation of the turbulent statistics of the flow.

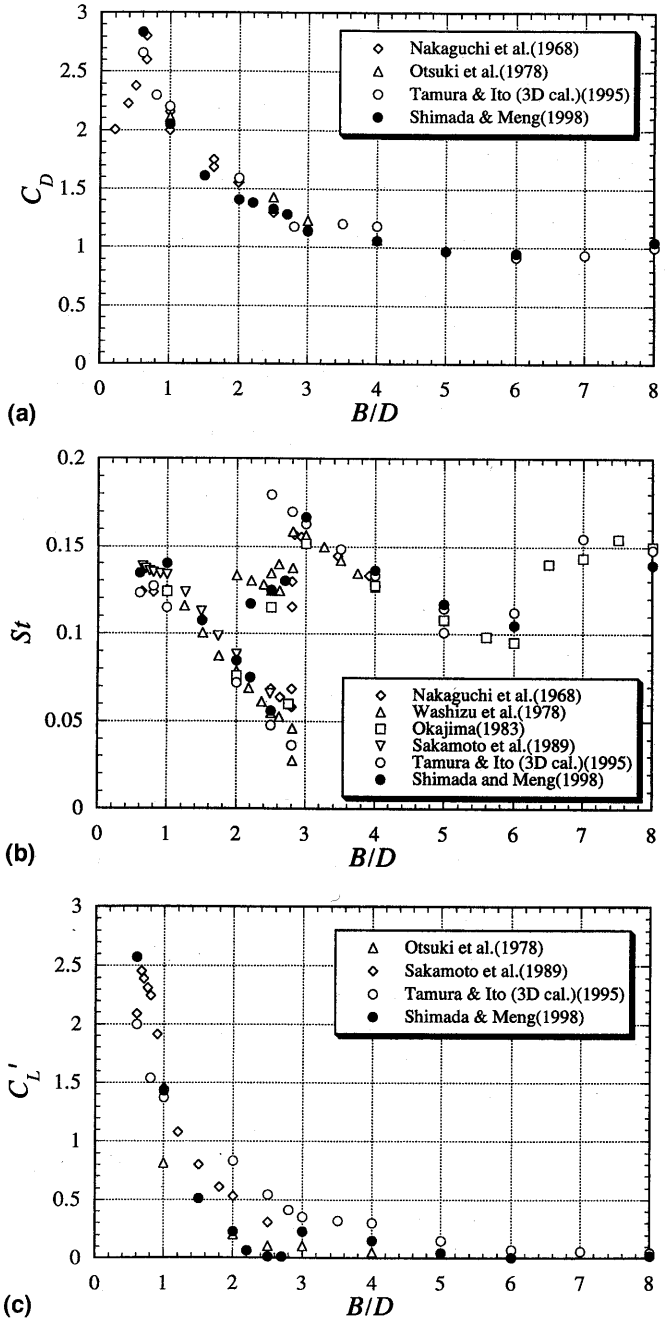

FIG. 12. Variations of Aerodynamic Characteristics According to *B/D* Ratio: (a) Mean Drag Coefficient; (b) Strouhal Number; (c) Fluctuating Lift Coefficient

Variation of Aerodynamic Characteristics with *B/D* Ratio

Fig. 12 shows the mean drag coefficient, the Strouhal number $St = nD/U_\infty$, and the fluctuating lift coefficient for changing B/D ratios. In the Strouhal number, frequency n is obtained from the predominant peaks observed in the spectrum of the lift. In the fluctuating lift coefficient, only the periodic component is considered. In these figures, wind tunnel experiment results (Nakaguchi et al. 1968; Otsuki et al. 1978; Washizu et al. 1978; Ohya et al. 1980; Okajima 1983) and results of a 3D numerical simulation (Tamura and Ito 1995) are presented for comparison. General features common to the measurements and analytical results are as follows.

The mean drag coefficient shows a peak near $B/D = 0.6$ and decreases monotonously as the B/D ratio increases. The Strouhal number exhibits discontinuities at $B/D = 2.8$ and near $B/D = 6.0$. Experimental data on the fluctuating lift coefficient available for comparison are limited, but they do show a tendency to decrease monotonously starting at $B/D = 0.6$. The results of the present numerical simulation are almost consistent with both the experimental results and those of 3D numerical analyses, in particular with respect to the mean drag coefficient and the Strouhal number. As for the fluctuating lift coefficient, the present numerical results are relatively small in value as compared with the results of the experiment and 3D analyses. This point will be discussed in more detail later.

Instantaneous vorticity contours are illustrated in Fig. 13 to show the flow pattern around the cross sections for the sake of understanding the aerodynamic statistics described above. In general, the results of an unsteady 3D analysis show small-

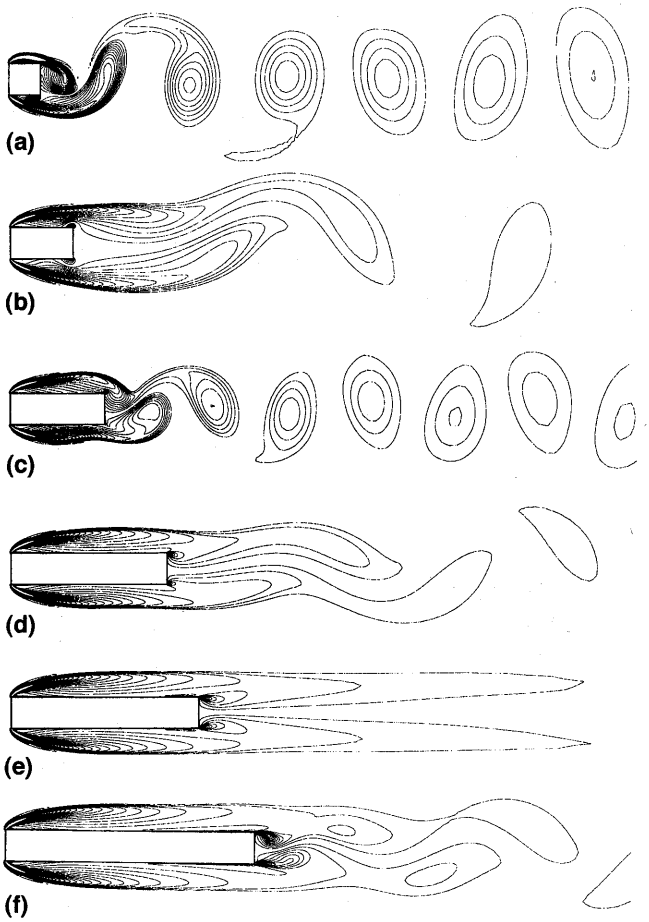

FIG. 13. Instantaneous Vorticity Contours around Rectangular Cross Sections with Various *B/D* Ratios at Maximum Lift: (a) *B/D* = 1.0; (b) *B/D* = 2.0; (c) *B/D* = 3.0; (d) *B/D* = 5.0; (e) *B/D* = 6.0; (f) *B/D* = 8.0

scale eddy structures due to the 3D turbulent motion in the vicinities of the boundaries of the cross sections. However, no such small-scale eddies are visible in the output of the present analysis, which uses the RANS model. This is because a perturbation such as small-scale eddies from the ensemble averaged fluctuation is regarded as turbulence numerically, which is incorporated as eddy viscosity in the equation; hence, such small-scale eddies are obscured by the turbulent viscosity effect.

Separated-Type Cross Sections (B/D < 2.8)

In the separated-type rectangular cross sections, a periodic and apparent vortex shedding can be observed, as illustrated in Figs. 13(a and b). Examining the mean pressure coefficient, it can be seen in Fig. 14 that there is no pressure recovery on the side surface for B/D = 1.0 and 2.0.

As the B/D ratio increases up to about B/D = 2.0, the location of the generation of the vortex behind the cross section moves further away from the cylinder and, coincidentally, the Strouhal number becomes smaller. Almost at B/D = 2.0, generation of the vortex behind the cross section becomes the weakest compared with other cross sections. Fig. 15 shows a comparison of the temporal mean streamlines for B/D = 2.0 as evaluated by the present numerical simulation and from detailed measurements by Mizota and Okajima (1981) using a tandem hot-wire anemometry. They showed that at B/D = 2.0, the reversed flow region is large and extends far away downstream of the cross section. Although the wake calculated by the present simulation is larger as compared with that measured by Mizota and Okajima, it does correspond qualitatively with the measured wake in that the reversed flow region extends downstream of the cross section.

Reattached-Type Cross Sections (2.8 < B/D ≦ 8.0)

At B/D = 3.0, the Strouhal number is reported to have a value between 0.16 and 0.17, so the vortex shedding period becomes small abruptly. This is well reproduced by the present numerical approach, which leads to a rapid increase in Strouhal number up to 0.167, at which time the space of the vortex shedding immediately becomes narrower and apparent vortex shedding appears again. Coincidentally, the fluctuating lift coefficient recovers, as seen in Fig. 12(c). A separation bubble is generated on the side surface of the cross section. The mean

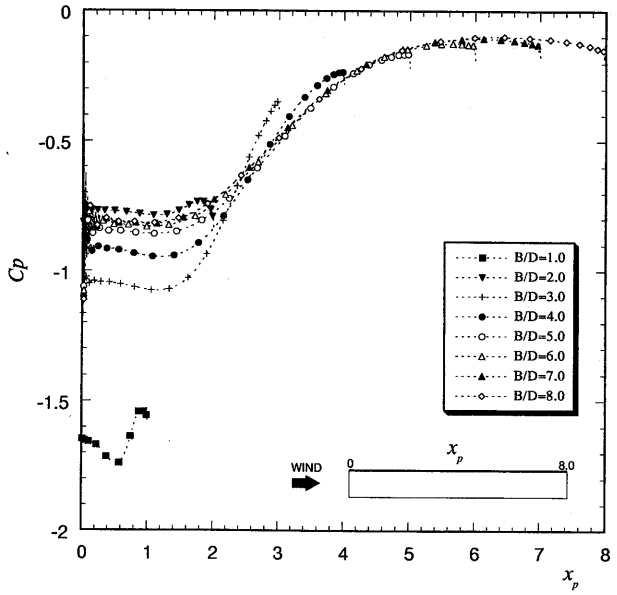

FIG. 14. Mean Pressure Distribution on Side Surface of Various *B/D* Ratios

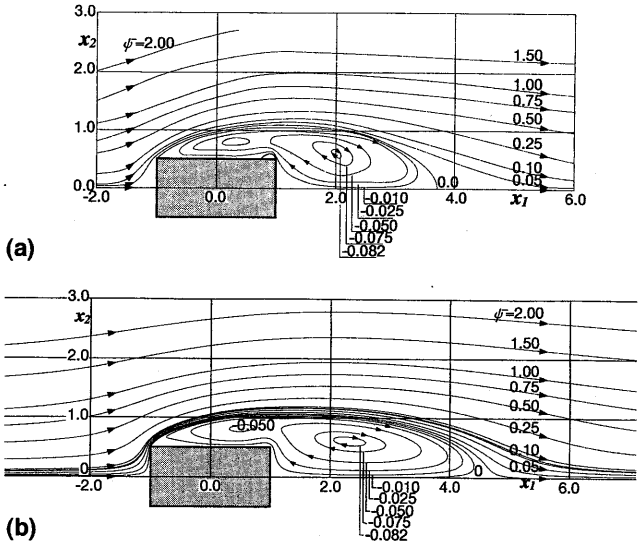

FIG. 15. Comparison of Time Mean Streamline of *B/D* = 2.0 Rectangular Cylinder: (a) Measurement by Mizota and Okajima (1981); (b) Result by Present Numerical Simulation

pressure coefficient is lower on the windward side surface and recovers on the leeward side, as seen in Fig. 14. Also, separation bubbles are alternately generated above and below the cross section. These tendencies are observed in every cross section almost up to B/D = 5.0. Fig. 16 shows an example of the periodical reattached-type cross section, for which a comparison of the time mean streamline is made between the results of the present numerical simulation and measurements conducted by Mizota et al. (1981). The result of the present simulation corresponds well with the measured data regarding the size of the separation bubble and that of the reversed flow region that is formed in the wake of the cylinder.

In Fig. 12(b), another discontinuity in Strouhal number can be recognized at B/D = 6.0. In the vorticity contour at B/D = 6.0 [Fig. 13(e)] evaluated by the present numerical analysis, though a weak motion of flow can be recognized in the wake far away from the section, flow near and around the cross section is almost close to being symmetrical; thus, its vortex shedding is apparently weak compared with that of other cross sections. At B/D = 8.0, the vortex resumes shedding from the trailing edge of the section, as can be seen in Fig. 13(f); thus, the Strouhal number increases again.

Mean pressure coefficients of reattached-type cross sections with 3.0 ≦ B/D ≦ 8.0 evaluated using the present numerical

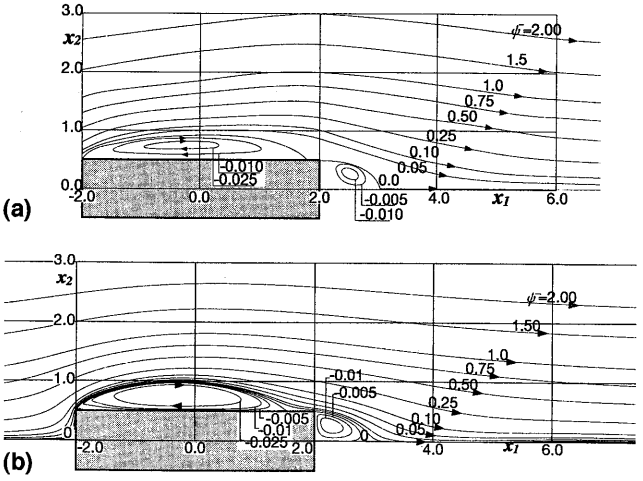

FIG. 16. Comparison of Time Mean Streamline of *B/D* = 4.0 Rectangular Cylinder: (a) Measurement by Mizota and Okajima (1981); (b) Result by Present Numerical Simulation

simulation show that the positions of the suction peak and of the pressure recovery are almost the same. Particularly over the range $5.0 \leqq B/D \leqq 8.0$, the distributions are almost identical and can be expressed by one distribution along the surface. This tendency corresponds well with the results of 3D calculations (Tamura and Ito 1995), although results are not presented here.

Fluctuating Lift Coefficient

In the ensemble-averaged model, in the case of flows with periodic unsteadiness, the instantaneous value of the physical quantity ϕ can be separated as follows (Reynolds and Hussain 1972; Franke and Rodi 1991):

$$\phi(t) = \bar{\phi} + \phi' = \bar{\phi} + \tilde{\phi} + \phi'' \tag{13}$$

where $\bar{\phi}$ = time-mean value; ϕ' = deviation from time-mean value; $\tilde{\phi}$ = periodic fluctuation; and ϕ'' = stochastic turbulent fluctuation. In the calculation of the unsteady RANS model, the ensemble averaged value, $\bar{\phi} + \tilde{\phi}$, is directly solved from the simulation. However, the stochastic component is evaluated as its variance. Thus, the variance of the total fluctuation is

$$\sigma_{\phi}^2 = \sigma_{\tilde{\phi}}^2 + \sigma_{\phi''}^2 \tag{14}$$

For example, in the unsteady calculation of the k-ε model, variance of the periodic component of velocity is evaluated as

$$\sigma_{\tilde{u}_i}^2 = \frac{1}{T}\int_0^T \tilde{u}_i^2(t)\, dt \tag{15}$$

The stochastic component of velocity is evaluated as its variance and is related to the turbulent kinetic energy k, which is solved from its transport equation as follows:

$$\sigma_{u_i''}^2 = \nu_t \left(\frac{\partial U_i}{\partial x_j} + \frac{\partial U_j}{\partial x_i}\right) - \frac{2}{3}k \tag{16}$$

However, for the pressure, its stochastic component is not modeled explicitly in any RANS model; therefore, its total fluctuation consists of the fluctuation only by $\tilde{p}$:

$$\sigma_{p_{\text{RANS}}}^2 = \sigma_{\tilde{p}}^2 < \sigma_{p_{\text{exact}}}^2 \tag{17}$$

Thus, its value is always underestimated, as compared with the exact value of its fluctuation. Since lift force is an integrated value of the surface pressure, the same argument holds in prediction of the lift fluctuation.

In separated-type cross sections, the periodic component of the lift produced by cross-stream flapping of the separated shear layer is predominant. Therefore, the results of the present numerical simulation, which takes into account only the periodical fluctuation, almost agrees with the results of experiment and 3D numerical results in which all components are included.

Cross sections with $1.5 < B/D < 3.0$ belong to the separated-type, but the location at which the Karman vortex is generated moves away from the cross section. Thus, as the cross-stream flapping of the separated shear layers becomes weak and the relative contribution of the periodic component to the total fluctuation becomes small, the fluctuating lift coefficient obtained by the present numerical simulation becomes smaller than the experimental results.

When the B/D ratio becomes larger and reattachment of the separated shear layer begins to occur, the relative contribution of the stochastic component to the total fluctuation becomes large. Therefore, as for reattached-type cross sections, a quantitative difference becomes noticeable. However, as there has been no research on the characteristics of the fluctuation in the aerodynamic forces by dividing it into periodic and stochastic components, it is difficult here to judge the validity of these arguments.

Aeroelastic Vibration of $B/D = 2.0$ Rectangular Cross Section

In this section, the applicability of the modified k-ε model is extended to the prediction of aeroelastic behavior of a $B/D = 2.0$ rectangular cross section based on its ability in simulating the aerodynamic behavior of stationary cross sections as described above. The aerodynamic characteristic of a stationary $B/D = 2.0$ rectangular cross section is classified as separated, but at the same time, it also belongs to the reattached category, because it shows unsteady reattachment onto the side surfaces. Therefore, this cross section exhibits both galloping and motion-induced vortex oscillation, which are typical of the separated-type and the reattached-type cross sections, respectively.

The unsteady wind force of the transversely forced oscillation is examined first. Expressing the displacement of the forced oscillation as $y_m(t) = \Re[Y_m \exp(i\omega_m t)]$, where Y_m and ω_m = amplitude and circular frequency of the forced oscillation, the frequency response part C_{L_m} can be decomposed as follows:

$$C_{L_m}(t) = \Re[(C_{L_R} + iC_{L_I}) \cdot e^{i\omega_m t}] \tag{18}$$

$$C_{L_R} = |C_{L_m}| \cdot \cos\beta_L, \quad C_{L_I} = |C_{L_m}| \cdot \sin\beta_L \tag{19}$$

$$|C_{L_m}| = \sqrt{C_{L_R}^2 + C_{L_I}^2}, \quad \beta_L = \tan^{-1}\left(\frac{C_{L_I}}{C_{L_R}}\right) \tag{20}$$

In Fig. 17, the simulated unsteady wind force is demonstrated,

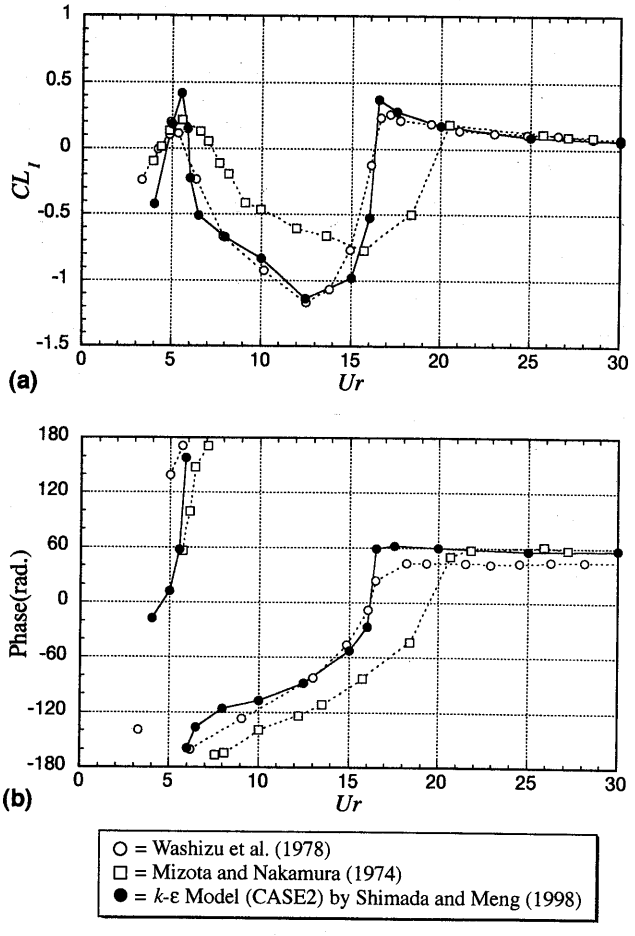

FIG. 17. Unsteady Aerodynamic Force of $B/D = 2.0$ Rectangular Cross Section (Heaving Amplitude: 0.1D): (a) CL_I; (b) Phase Lag β

which corresponds to the forced oscillation in the heaving mode with an amplitude of $0.1D$. C_{L_I} becomes positive in the region near $Ur = 5$ and $Ur > 15$, at which a motion-induced vortex oscillation and Karman vortex-induced vibration occur, respectively. The computed results are in good agreement with the experimental results (Washizu et al. 1973; Mizota and Okajima 1975). The response amplitude of the vortex-induced oscillation is dependent on the Scruton number; however, in the galloping it is dependent also on the mass ratio according to the quasi-steady theory (Parkinson 1964). Therefore, to compare the results in the regions from the vortex-induced vibration to the galloping, both mass ratio and damping decrement should be provided. Those parameters in the present calculation are set as indicated in Table 3, and the computed results are compared with the experimental results, whose mechanical parameters are also included in the same table. In Fig. 18 the elastically supported response is demonstrated by examining the relation between the reduced velocity and the normalized amplitude (Y/D).

At $Ur = 5.5$, the motion-induced vortex oscillation is at its maximum amplitude of $Y/D = 0.175$. At this time, the lift fluctuation is sinusoidal, as shown in Fig. 19(a). The base pressure and mean drag at this reduced velocity is larger than those at rest. This is because of the existence of the secondary vortex, which is formed at the trailing edges of the cross section, as can be seen in Fig. 20(a). This vortex becomes coalesced with the rolled-up vortex traveling downstream along the side surfaces from the leading edge and is shedded into the wake. The flow pattern is seen to be completely synchronized with the motion of the cylinder. At $Ur = 6.0$, vortex shedding is no longer synchronized, and the amplitude decreased abruptly. The response resumes increasing its amplitude at a value of Ur of about 12.0. At $Ur = 15.0$, the reduced velocity almost coincides with the resonant velocity, which is defined as the reciprocal of the Strouhal number $St = 0.085$. Since the natural frequency is close to the frequency of the Karman vortex shedding, the oscillation is found to be modulated, as can be seen in Fig. 19(b). The envelope of modulation in the time history

TABLE 3. Mechanical Parameter of Vibrating Cylinder

Source (1)	Sc (2)	Mass ratio (3)	Logarithmic damping (4)
Takeda and Kato (1992)	1.6	302	0.0053
Miyazaki (1982)	3.0	750	0.0040
Present calculation	2.0	500	0.0040

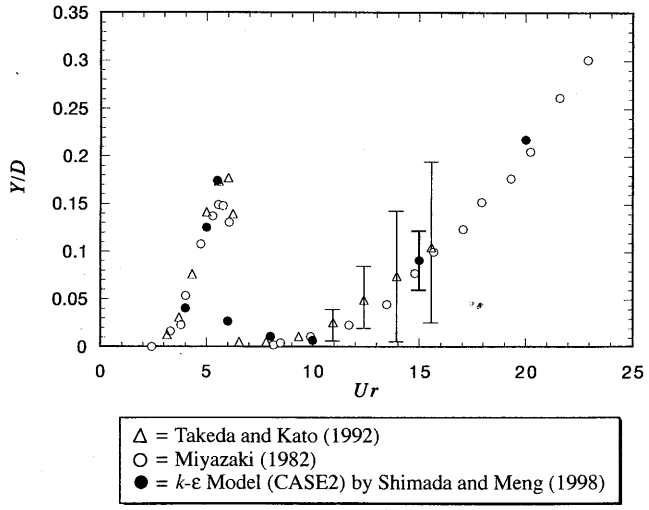

FIG. 18. Aeroelastic Vibration of $B/D = 2.0$ Rectangular Cross Section (Heaving Motion)

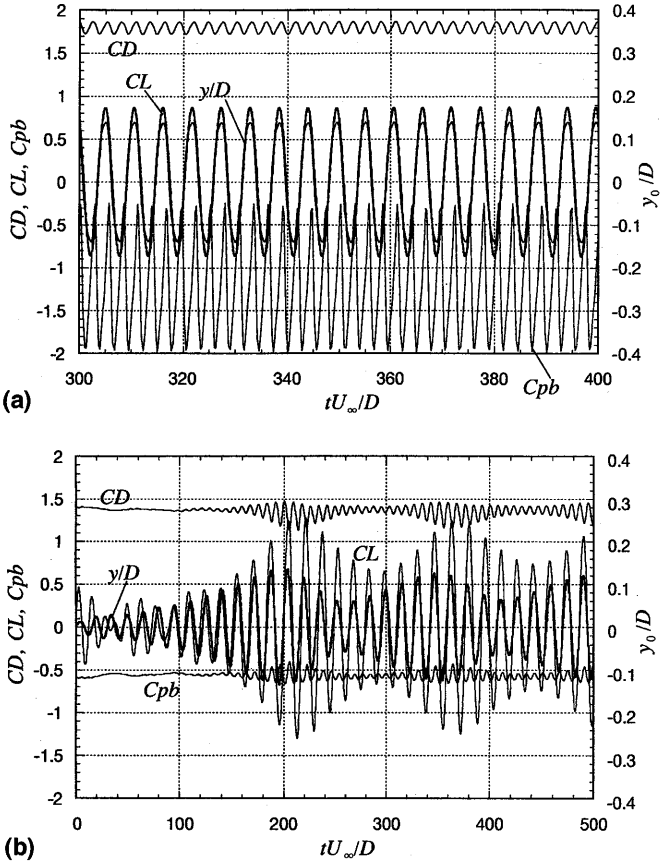

FIG. 19. Aerodynamic Forces and Response of Transversely Oscillating $B/D = 2.0$ Rectangular Cross Section: (a) $Ur = 5.5$; (b) $Ur = 15.0$

is indicated by the error bars in Fig. 18. Takeda and Kato (1993) also reported a similar type of modulation in the same reduced velocity region from observations of experiments. At $Ur = 20.0$, the oscillation becomes sinusoidal again with an amplitude of $Y/D = 0.21$. This amplitude is in good agreement with the experimental result. Since the Scruton number is relatively small in value, the vortex-induced vibration, which starts at Ur of almost 12.0, is seen to develop directly into the galloping mode without any decrease in its amplitude, as reported for a square prism by Parkinson and Wawzonek (1981). At this reduced velocity, the flapping of the separated shear layer becomes important, as seen in Fig. 20(b).

Thus, the k-ε model showed quite satisfactory results when the cross section is vibrating, although at rest prediction of lift, fluctuation is considerably underestimated. This is because when the cross section begins to vibrate, lift fluctuation may

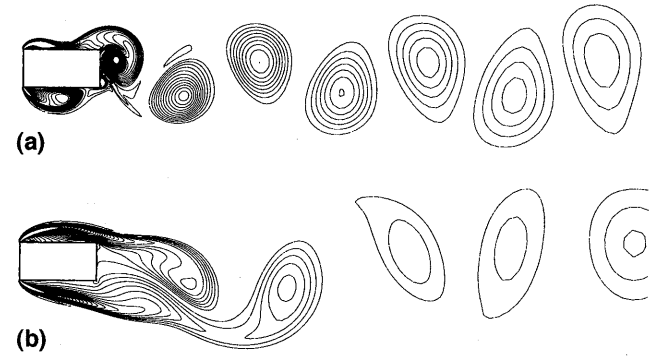

FIG. 20. Instantaneous Vorticity Contour of Vibrating $B/D = 2.0$ Rectangular Cross Section in Heaving Mode at Maximum Amplitude: (a) $Ur = 5.5$; (b) $Ur = 20.0$

be dominanted by the periodic component, and contribution of the stochastic component becomes negligible.

CONCLUSIONS

In this paper, prediction of aerodynamic characteristics of bluff bodies are reviewed. First, direct numerical simulation was demonstrated. In this method, 3D treatment was necessary; however, in a few cases the 2D version of the method was successful in predicting characteristics such as motion-induced, vortex-induced vibration.

Extensive research on the k-ε model has shown that it is possible to apply the model to evaluation of the flow past a square cross section by introducing eddy viscosity to incorporate the three-dimensionality effect, namely, the spanwise momentum diffusion. However, so far the application of this model has been made only for square cross sections. In the present study, this model was applied to a wider range of cross sections in order to extend its applicability. As a result, well-organized coherent vortical structures were successfully simulated for all of the analyzed cross sections, and simulated various typical aerodynamic features were in good agreement with experimental results, particularly for discontinuities in the Strouhal number at the critical sections of B/D = 2.8 and 6.0. Consequently, it was shown that this model was, in fact, also applicable to rectangular cross sections for a considerably wide range of B/D ratios.

An incompleteness of the ensemble-averaged model was also recognized by this study. The prediction of lift fluctuation was considerably underestimated in some cases for stationary cross sections when compared with the experimental results. This is due to a defect in the turbulence model, which cannot evaluate the stochastic component of pressure fluctuation.

On the other hand, the model showed quite good features for prediction of the unsteady force of transversely forced oscillation and elastically supported vibration. In this sense, the k-ε model is expected to be a quite suitable method for these kinds of aeroelastic applications.

APPENDIX I. REFERENCES

Bearman, P. W., and Obasaju, E. D. (1982). "An experimental study of pressure fluctuations on fixed and oscillating square-section cylinders." *J. Fluid Mech.*, 119, 297–321.

Bosch, G., and Rodi, W. (1998). "Simulation of vortex shedding past a square cylinder with different turbulence models." *Int. J. Numer. Methods in Fluids*, 28, 601–616.

Deng, G. B., Piquet, J., and Visonneau, M. (1994). "2-D computations of unsteady flow past a square cylinder with the Baldwin-Lomax model." *J. Fluids and Struct.*, 8, 663–680.

Franke, R., and Rodi, W. (1991). "Calculation of vortex shedding past a square cylinder with various turbulence models." *Proc., 8th Symp. on Turbulent Shear Flows*, Technical University of Munich, Munich, Germany, 20–21.

Harlow, F. H., and Welch, J. E. (1965). "Numerical calculation of time-dependent viscous incompressible flow of fluid with free surface." *Phys. Fluids*, 8, 2182–2189.

Kato, M. (1997). "2-D turbulent flow analysis with modified k-ε around a stationary square cylinders and vibrating one in the along and across wind direction." *J. Struct. Mech. Earthquake Engrg.*, 577(I-41), 217–230.

Kato, M., and Launder, B. E. (1993). "The modeling of turbulent flow around stationary and vibrating square cylinders." *Proc., 9th Symp. on Turbulent Shear Flows*, Kyoto, Japan, 8.

Kawamura, T., and Kuwahara, K. (1984). "Computation of high Reynolds number flow around circular cylinder with surface roughness." American Institute of Aeronautics and Astronautics, Reston, Va., Paper 84-0340.

Komatsu, S., and Kobayashi, H. (1980). "Vortex induced oscillation of bluff cylinders." *J. Wind Engrg. and Industrial Aerodyn.*, 6, 335–362.

Lee, B. E. (1975). "The effect of turbulence on the surface pressure field of a square prism." *J. Fluid Mech.*, 69, 263–282.

Lee, S. (1997). "Unsteady aerodynamic force prediction on a square cylinder using k-ε turbulence models." *J. Wind Engrg. and Industrial Aerodyn.*, 67–68, 79–90.

Lyn, D. A. (1989). "ERCOFTAC Database Case 43." *Proc., 23rd Cong. Int. Assoc. Hydr. Res.*, International Association for Hydraulic Research, Delft, The Netherlands.

Miyata, T., Miyazaki, M., and Yamada, H. (1983). "Pressure distribution measurements for wind induced vibrations of box girder bridges." *J. Wind Engrg. and Industrial Aerodyn.*, 14, 223–234.

Miyazaki, M. (1982). "Suppression of wind oscillation of long span box girder decks—view from characteristics of pressure in motion." *Proc., 7th Nat. Symp. on Wind Engrg.*, Japan Association for Wind Engineering, Tokyo, 187–194.

Mizota, T., and Nakamura, Y. (1974). "Wind tunnel blockage effects on drag coefficient and wind-induced vibration." *Proc., 3rd Symp. Wind Effects on Struct.*, 210–208.

Mizota, T., and Okajima, A. (1981). "Experimental studies of unsteady flows around rectangular prisms." *Proc., Japan Soc. of Civil Engrs.*, Japan Society of Civil Engineers, Tokyo, 312, 39–47.

Murakami, S., Mochida, A., and Hayashi, Y. (1990). "Examining the k-ε model by means of a wind tunnel test and large-eddy simulation of the turbulence structure around a cube." *J. Wind Engrg. and Industrial Aerodyn.*, 35, 87–100.

Nagao, F., and Utsunomiya, H. (1988). "The validity of sectional models on wind tunnel tests for vortex induced oscillation of bridges." *J. Wind Engrg. and Industrial Aerodyn.*, 29, 351–360.

Nakaguchi, H., Hashimoto, K., and Muto, S. (1968). "An experimental study on aerodynamics drag of rectangular cylinders." *J. Japan Soc. of Aeronautical and Space Sci.*, Tokyo, 16(168), 1–5.

Norris, L. H., and Reynolds, W. C. (1975). *Rep. No. FM-10*, Dept. of Mech. Engrg., Stanford University, Stanford, Calif.

Ohya, A., Washizu, K., Fujii, K., and Otsuki, Y. (1980). "Wind tunnel experiments on aerodynamic forces and pressure distributions of rectangular cylinders in a uniform flow (part 2)." *Proc., 5th Symp. on Wind Effects on Struct.*, 153–160.

Okajima, A. (1983). "Flow around a rectangular cylinder with a series of various width/height ratios." *J. of Wind Engrg.*, 17, 1–19.

Otsuki, Y., Fujii, K., Washizu, K., and Ohya, A. (1978). "Wind tunnel experiments on aerodynamic forces and pressure distributions of rectangular cylinders in a uniform flow." *Proc., 5th Symp. on Wind Effects on Struct.*, 169–176.

Parkinson, G. V. (1964). "The square prism as an aeroelastic non-linear oscillator." *Quarterly J. Mech. and Appl. Mathematics*, 17(2), 225–239.

Parkinson, G. V., and Wawzonek, M. A. (1981). "Some considerations of combined effects of galloping and vortex resonance." *J. Wind Engrg. and Indus. Aerodyn.*, 8, 135–143.

Pocha, J. J. (1971). "On unsteady flow past cylinders of square cross-section," PhD thesis, Dept. of Aeronautics, Queen Mary College, London.

Reynolds, W. C., and Hussain, A. K. M. F. (1972). "The mechanics of an organized wave in turbulent shear flow. Part III: Theoretical models and comparisons with experiments." *J. Fluid Mech.*, 54, 263–288.

Rodi, W. (1991). "Experience with two-layer models combining the k-ε model with a one-equation model near the wall." *Proc., 29th Aerosp. Sci. Mtg.*, American Institute of Aeronautics and Astronautics, Reston, Va., Paper 91-0216.

Sakamoto, H., Haniu, H., and Kobayashi, Y. (1989). "Fluctuating force acting on rectangular cylinders in uniform flow (On rectangular cylinders with fully separated flow)." *Trans., JSME Ser. B.*, Tokyo, 55(516), 2310–2317.

Shimada, K. (1995). "Numerical analysis for the vortex-induced oscillation of prism with an elongated rectangular cross section (motion-induced vortex oscillation of 2D prism with B/D = 2 cross section)." *Trans., JSME Ser. C.*, Tokyo, 61(585), 1776–1783.

Shimada, K., and Meng, Y. (1997). "Two-dimensional numerical analysis for a circular cylinder in the uniform flow by the k-ε model." *Summaries of Technol. Papers of Ann. Meeting Arch. Inst. of Japan*, Architectural Institute of Japan, Tokyo, B-1, 327–328.

Shimada, K., and Meng, Y. (1998). "Applicability of modified k-ε model on the estimation of aerodynamic properties of rectangular cylinders with various elongated cross sections." *J. Struct. Constr. Engrg.*, Tokyo, 514, 73–80.

Shiraishi, N., and Matsumoto, M. (1982). "On vortex-induced oscillations of bluff cross sections used for bridge structure." *Proc., Japan Soc. of Civil Engrs.*, Japan Society of Civil Engineers, Tokyo, 322, 37–50.

Shiraishi, N., and Matsumoto, M. (1983). "On classification of vortex-induced oscillation and its application for bridge structures." *J. Wind Engrg. and Industrial Aerodyn.*, 14, 419–430.

Takeda, K., and Kato, M. (1992). "Wind tunnel blockage effects on drag coefficient and wind-induced vibration." *J. Wind Engrg. and Industrial Aerodyn.*, 42, 897–908.

Tamura, T., and Ito, Y. (1995). "Three-dimensional simulation of flow

and pressure around an elongated rectangular cylinder." *J. Struct. Constr. Engrg.*, Tokyo, 41–48.
Tamura, T., and Ito, Y. (1997). "Three-dimensional vortical flows around a bluff cylinder in unstable oscillation." *J. Wind Engrg. and Industrial Aerodyn.*, 67–68, 141–154.
Tamura, T., and Kuwahara, K. (1992). "Numerical study on aerodynamic instability of oscillating rectangular cylinders." *J. Wind Engrg. and Industrial Aerodyn.*, 41–44, 253–254.
Tamura, Y., and Shimada, K. (1987). "A mathematical model for the transverse oscillations of square cylinders." *Int. Conf. on Flow Induced Vibrations*, Institution of Mechanical Engineers, London, 267–275.
Utsunomiya, H., Nagao, F., and Hatakeyama, K. (1984). "Some investigations on the wind tunnel test of the aerodynamic behaviors of bluff bodies." *Proc., 8th Nat. Symp. on Wind Engrg.*, Japan Association of Wind Engineering, Tokyo, 327–332.
Washizu, K., Ohya, A., Otsuki, Y., and Fujii, K. (1978). "Aeroelastic instability of rectangular cylinders in a heaving mode." *J. Sound and Vibration*, 59(2), 195–210.
Wilkinson, R. H. (1974). "On the vortex-induced loading on long bluff cylinders," PhD thesis, Facul. of Engrg., University of Bristol, Bristol, U.K.
Yamada, H., Miyata, T., and Yamashita, Y. (1982). "Distorted vortex excitation of rectangular cylinders in heaving motion with angle of attack." *Proc., 7th Nat. Symp. on Wind Engrg.*, Japan Association for Wind Engineering, Tokyo, 243–250.

APPENDIX II. NOTATION

The following symbols are used in this paper:

B = streamwise length of cross section;
Cp = mean pressure coefficient [$=P/(1/2\rho_a U_\infty^2)$, where P = mean pressure];
Cp' = fluctuating pressure coefficient [$=\sigma_p/(1/2\rho_a U_\infty^2)$, where σ_p = standard deviation of pressure];
Cp_b = base pressure coefficient;
C_D = mean drag [$=F_D/(1/2\rho_a U_\infty^2 D)$, where F_D = mean drag per unit length];
C_L' = fluctuating lift coefficient [$=\sigma_L/(1/2\rho_a U_\infty^2 B)$, where σ_L = standard deviation of lift per unti length];
D = depth of cross section;
h = damping decrement;
k = turbulent kinetic energy;
m = mass per unit length;
n_0 = natural frequency;
P_k = production of turbulent kinetic energy;
p = pressure;
R = Reynolds number ($=U_\infty D/\nu$);
R_y = turbulent Reynolds number ($=k^{1/2}y/\nu$, where y = distance from wall);
Sc = Scruton number [$=2m/(\rho_a BD)\cdot 2\pi h$];
St = Strouhal number ($=n_\eta/U_\infty$ where n = peak frequency of lift);
U_i = ensemble averaged velocity (i = 1, 2);
Ur = reduced velocity ($=U_\infty/n_0 D$);
U_∞ = velocity at inlet boundary;
Y = displacement;
ε = dissipation rate of turbulent kinetic energy;
κ = Karman constant (=0.41);
ν_t = turbulent viscosity; and
ρ_a = air density.